Experimental characterization of monumental brick masonry in Nepal

Rishi Ram Parajuli[1], Aiko Furukawa[2], Dipendra Gautam[3, *]

[1]Department of Civil Engineering, University of Bristol, UK

[2]Department of Urban management, Kyoto University, Kyoto, Japan

[3]Department of Architecture and Civil Engineering, City University of Hong Kong, Kowloon, Hong Kong

*Corresponding author email: dip.gautam@my.cityu.edu.hk

Abstract

Mechanical properties of masonry play important role in the identification of seismic behavior during earthquakes. As historical earthquakes precisely note that the non-engineered masonry buildings are the most affected structural forms during earthquakes, analytical models should be more representative to capture the real damage mechanisms. Similar scenario was reflected during the 1988, 2011, and 2015 earthquakes in Nepal. However, an extensive literature survey noted that the mechanical properties of Nepali masonry construction are still not well identified and thus require due attention to improve numerical models. To this end, this study aims to identify the mechanical properties for neoclassical monumental masonry constructions in Nepal. In-situ tests, analytical validation using discrete element modeling, and laboratory test results are reported in this paper.

Keywords: Mechanical property; brick masonry; mud mortar; monumental construction; Nepal.

Introduction

Masonry structures comprise the largest fraction of building worldwide and their existence will continue for centuries due to socio-economic constraints, cultural affinity, economic viability, resource availability, among others. Masonry construction comprises monumental, administrative, and residential structures. Seismic vulnerability of residential construction higher than that of the monumental constructions due to associated inferiorities in terms of workmanship, technology, materials, and periodic repair and maintenance. Heritage structures encapsulate history and reflection of construction technology thus they require periodic strengthening for conservation (Tamrakar & Parajuli, 2019). The damage incurred during the 1934 and 2015 earthquakes in Nepal firmly outline very high vulnerability of Nepali monumental constructions (Gautam, 2017). Despite this, more than 60% of the residential buildings are either stone or brick masonry constructions in mud mortar in Nepal (Central Bureau of Statistics, 2012) and their seismic performance would gravely alter the damage and loss statistics. To this end, seismic assessment of masonry structures in Nepal requires due attention in terms of experimental and analytical studies. For more representative analytical models, mechanical characterization is very important as the parameter values may alter the performance level. Structural evaluation of existing structures gravely depends on the realistic material properties and the use of numerical methods. Thus, experimentally estimated material properties are backbone for reliable numerical analyses. Many researchers have experimentally characterized the properties of masonry prisms and masonry units for different types of masonry construction systems (see e.g. Costigan, Pavía, & Kinnane, 2015; Jafari, Rots, Esposito, & Messali, 2017; Kaushik, Rai, & Jain, 2007; Sarangapani, Reddy, & K. S., 2005; Parajuli & Kiyono, 2015; Parajuli, 2020). The properties of masonry buildings in New Zealand were determined by using field and laboratory tests (Lumantarna, Biggs, & Ingham, 2014b, 2014a). Similarly, material properties of ancient structures in Iran were reported together with few combinations of mortar ratios by Rahgozar & Hosseini (2017). These studies provide an important basis to delineate the likely performance of masonry structures during earthquakes. However, due to the variation in type, manufacturing process, and constituents, mechanical properties of masonry from one region will not be the same for another. Although being widely recognized as one of the most active seismic regions in the world, studies related to masonry constructions are limited in Nepal. Some numerical and forensic interpretation based studies have emerged in the recent decades (e.g. (Gautam, 2017); (Gautam & Rodrigues, 2018)); however, experimental studies have not surfaced widely (e.g. (Adhikari, Jha, Gautam, & Fabbrocino, 2019)). Owing to the frequent seismic activities throughout the Himalayan arc, seismic safety of masonry buildings has emerged as a great concern throughout the Hindu Kush Himalayan region. However, limited works could be found throughout the region (see e.g.(Ali et al., 2013); (Ahmad, Ali, Ashraf, Alam, & Naeem, 2012); (Ahmad, Ali, & Umar, 2012); (Gautam, 2018); (Adhikari et al., 2019); among others). It is obvious that the wide discrepancies in construction workmanship and materials may lead to a greater variation in properties of materials; thus, more dedicated studies are required for each masonry type, preferably in local scale.

Most of the neoclassical buildings constructed during the 19th century in Nepal are now considered as heritage assets although they were fundamentally constructed for residential and administrative purposes. Materials used in such buildings were especially manufactured for neoclassical constructions. The neoclassical monuments have peculiar specifications in terms of materials such as brick masonry in mud mortar or brick masonry in *Surkhi*-lime mortar (brick powder and lime mortar). Further details regarding the construction systems and details of the structural and architectural components regarding neoclassical monuments are reported by Adhikari et al. (Adhikari et al., 2019). A broad literature review highlighted that experimental studies on mechanical properties of monumental brick masonry from developing countries such as Nepal are quite limited.

However, studies on mechanical characterization of monumental constructions are abundantly reported especially in southern Europe (see e.g. (Formisano, Vaiano, Fabbrocino, & Milani, 2018), (Potenza et al., 2015), (Barluenga et al., 2014); (Boschi, Galano, & Vignoli, 2019), (Milosevic, Gago, Lopes, & Bento, 2013), among others). To fulfill this hiatus, we conducted laboratory and in-situ tests in some brick masonry wallets, brick masonry units, and mud mortar that is commonly used as the binding agent in monumental brick masonry constructions.

Materials and Methods

We collected samples from two monumental structures, viz. Shreemahal and Singh Durbar. Both structures are located in Kathmandu Valley and were damaged by the 2015 Gorkha earthquake. Brick samples were collected from the monuments and tested on different dates. Laboratory test for brick, direct compression, and shear strength of brick masonry wall was conducted in the Central Materials Testing Laboratory (CMTL) and Heavy Lab at Institute of Engineering (IOE), Pulchowk Campus and Civil Engineering Lab (CEL), Institute of Engineering (IOE), Thapathali Campus.

Brick test was conducted using the Compression Testing Machine (CTM) and Universal Testing Machine (UTM) at CMTL and CEL. The wallet tests were performed at the CMTL and the Heavy Lab at IOE Pulchowk Campus. The samples were prepared following the procedure suggested by the Indian standard (IS) IS 3495-1 (Bureau of Indian Standards, 1992). Once the samples were prepared, surfaces were smoothened, and the specimens were soaked in water for 24 hours. The frogs and other gaps of the specimens were filled with a cement sand mortar (1:3) and sand only. Bricks were then wrapped in a damp jute bag for 24 hours and immersed for three days in clean water. The load was gradually increased, and corresponding displacements were recorded. We also collected specimens from the wall for shear test, compressive strength test, and particle distribution test following standard test procedures. Compression test and shear test of the masonry wallets with mud mortar were performed at CMTL. All the materials required for the preparation of the sample were extracted from partially collapsed Shreemahal monument. Walls with the required sizes to fit on the testing apparatus were prepared on the metal baseplates. Four wall models were prepared for compressive strength test of the wallets. The dimension of the wallets was 360 × 360 × 340 mm. All the samples were prepared in English bond with mud mortar of thickness ~12 mm to replicate the real construction scenario in monumental constructions. The top surface of the samples was smoothened and leveled by mud plaster. The walls were left in room temperature to dry for 28 days. Sand was used to level the top surface of the walls and metal plates were stacked above the sand layer to assure a uniform distribution of vertical loads. The load was increased gradually, and respective displacements were recorded for each increment.

Brick elements taken from Shreemahal were used to prepare the walls of size 900×900 ×450 mm. Clay was collected from the quarry sites where similar clay that was used for the monumental construction was abundant. However, it should be noted that even careful estimation, approximation, and preparation of properties and sample may not lead to the exact scenarios. This is due to the fact that technologies and skills may have drifted significantly over these decades and exact replication may not be possible due to lack of knowledge on how the original structure was planned and constructed. Skilled masons with prior experience were hired to prepare the wallets. Clay was kept wet for about 24 hours to assure thorough mixing of water in it and to have a good bond. Four walls were prepared on metal baseplates in the lab and were kept in room temperature for 28 days. Test setup for the shear test was arranged in such a way that the target forces and measurement of displacements would be achieved. Fig. 1 shows some evidence of the experimental campaign conducted at the Heavy Lab at Institute of Engineering, Pulchowk Campus, Nepal. A wall panel and loading directions are shown in Figs. 2a and 2b. Constant vertical load was applied at the top of the wall and monotonic lateral load was applied gradually up to the failure point. The horizontal load was applied at the two third of the height of the wall, i.e. 600 mm from the bottom of the wall. Four samples were tested with varying constant vertical loads of 10, 12, 15, and 18 KN, meanwhile, displacements in each load increment was recorded.

Fig. 1 a) and b) Loading arrangement for masonry wallet, c) crack initiation in wallet, d) cracked specimen, e) specimen contained by metal plates, f) and g) cracks propagated in masonry wallets

Fig. 2 a) Experimental setup for in-plane shear test showing loading direction, b) wall samples prepared for in-plane shear test

Shove test, a semi-destructive way of testing the masonry strength in-situ, was used to test the shear strength of masonry walls in Singh Durbar. A calibrated hydraulic ram capable of displaying applied load was used together with a dial gauge for in-situ tests. The dial gauge position was maintained by drilling holes on the wall. Test location was prepared by removing the brick on sides of the target brick unit including the mortar on one side of the brick to be tested. The head joint on the opposite side of the brick to be tested was also removed. We assured that the mortar joints above and below the test brick remain undisturbed. The hydraulic ram was then inserted in the space from where the brick was removed. A steel loading block was placed between the ram and the brick to be tested so that the ram would distribute its load over the end face of the brick. The dial gauge was also placed to record the displacement to obtain the force-deflection plot. The brick was then loaded with the ram till the indication of cracking or movement of the brick first appears. The ram force and associated deflection on the dial gauge were recorded. The joint was inspected for estimation of effective joint area to resist the force from the ram. The in-situ shear strength test was carried out at the main building of Singh Durbar at five different locations. Three tests were conducted on the ground floor and the other two were conducted on the first floor.

Results

Compressive strength of bricks

The compressive strength test results for the bricks from Shreemahal are summarized in Table 1. As shown in Table 1, average compressive strength of brick is found to be 6.40 MPa and average -water absorption ratio is obtained as 15.98%. The summary of the compressive strength of bricks is presented in Table 2. Comparison between Table 1 and Table 2 highlights that the bricks with frogs filled with sand have lower compressive strength when compared with the bricks with frog filled with cement mortar. This is due to the fact that cement mortar has better strength and thus resists greater load. The sand usually gets displaced when loaded so the strength of brick is obtained to be lower in this case. In the case of frog filled with cementitious materials, the load will be acting on the stiffer element hence alters the value of the compressive strength. The summary of the compressive strength of bricks from Singh Durbar is presented in Table 3. The average compressive strength is obtained as 19.89 MPa, which is very high when compared to the normal bricks that are available in the market nowadays. Similarly, the load displacement plot was obtained using the test results as shown in Fig. 3. Fig. 3 shows the variation in displacement upon load for nine brick samples. The bricks were not machine-made bricks thus their constituents usually vary, and the manufacturing process would also vary. This leads to the variation in displacement. The sudden drops in the curves in Fig. 3 highlight the initiation of cracks in the sample.

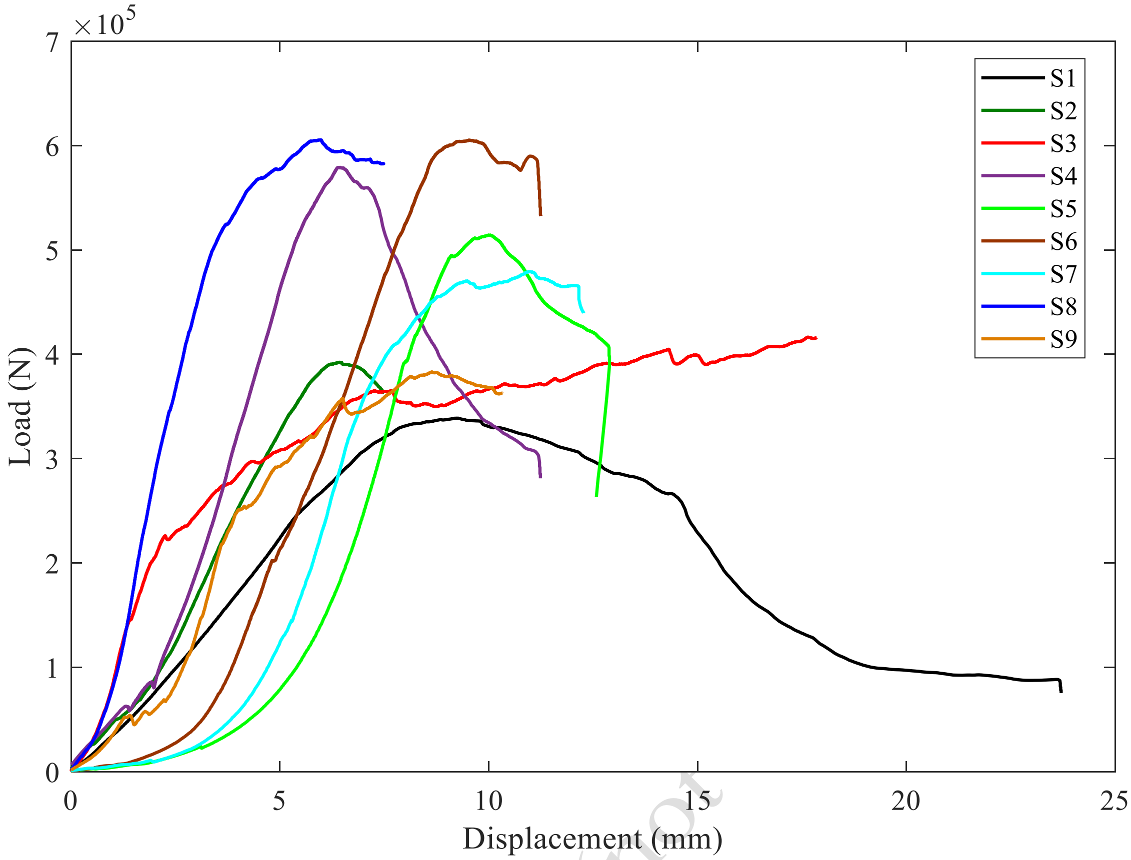

Fig. 3 Breaking load vs. displacement plot for the Singh Durbar brick samples

Table 1. Compressive strength of brick from Shreemahal (frog filled with cement mortar)

Brick Sample No.	1	2	3	Average
Dimension (L×B×H) mm	230×115×70	232×116×70	228×115×70	230×115.33×70
Breaking load (N)	202000	182000	126000	170000
Breaking strength (MPa)	7.64	6.76	4.81	6.40
Water absorption (%)	13.00	17.25	17.69	15.98

Table 2. Compressive strength of brick from Shreemahal (frog filled with sand)

Sample no.	Length (mm)	Breadth (mm)	Breaking load (N)	Compressive Strength (MPa)
S1	230	119	100000	3.65
S2	230	117	100000	3.72
S3	230	117	94000	3.49
S4	235	119	110000	3.93
S5	230	114	120000	4.58
S6	230	115	174000	6.58
	Average			4.33

Table 3. Compressive strength of brick from Singh Durbar (frog filled with cement mortar)

Sample no.	Length (mm)	Breadth (mm)	Breaking load (N)	Compressive Strength (MPa)
S1	245	110	338768.4	12.57
S2	222	105	392321.1	16.83
S3	227	111	416352.2	16.52
S4	211	102	579043.9	26.90
S5	232	104	514110.6	21.31
S6	234	108	605198.0	23.95
S7	223	103	479137.7	20.86
S8	221	110	605354.8	24.90
S9	241	105	383171.3	15.14
	Average			19.89

The average compressive strength of brick from Singh Durbar is found to be 19.89 MPa when the frog was filled with cement mortar. Adhikari et al. (Adhikari et al., 2019) reported the maximum compressive strength of Bagh Durbar monument as 6.63 MPa. Similarly, Jha et al. (Jha, Motra, Sah, Adhikari, & Gautam, 2019) reported the maximum compressive strength from Bal Mandir monument was ~ 15 MPa. This highlights that the monumental brick masonry units were especially manufactured and have considerably high compressive strength. Usually, bricks having 7.5 MPa strength are regarded as first-class bricks in Nepal and the average compressive strength of Singh Durbar bricks show that they are very high-quality bricks despite being more than 80 years old. It is worthy to note that the bricks were manufactured many decades ago, and their initial compressive strength may be different than the value obtained in this test.

Wallet test

The compressive strength test results for four brick masonry walls in mud mortar are summarized in Table 4. Similarly, compressive strength and modulus of elasticity are presented in Table 5. The stress-strain relationships for all the samples are shown in Fig. 4. The average compressive strength of the brick wall and the modulus of elasticity are found to be 0.865 MPa and 29.145 MPa respectively. The observed failure pattern closely represents the likely failure pattern due to earthquake loading. The summary of shear strength test results is presented in Table 6. Equivalent coulomb parameters ‘c’ and ‘φ’ for the masonry wall panel are found to be 0.024 MPa and 16.98 degrees for brick masonry in mud mortar. The variation in the compressive strength of brick masonry walls depends on several factors such as thickness of mortar remaining water content inside the wall specimen, handling of the samples before testing, among others.

The major factor that affects the compressive strength value is the use of masonry wall cubes without lateral restraints (Sarangapani et al., 2005). In the case of low strength mortars, load applied at the top of the wall starts to push laterally in each step of loading in lower layers. Low shear strength in joints results spreading of the bricks laterally which leads to the failure of the specimen with much deflection even though the metal plates are used at the top to distribute loads uniformly. Laterally restrained prisms in two opposite faces would lead to a better result in compression test of low strength masonry.

Table 4. Summary of stress-strain values recorded during compression strength test of masonry walls with mud mortar

Step	Sample No 1 (S1)		Sample No 2 (S2)		Sample No 3 (S3)		Sample No 4 (S4)	
	Stress (MPa)	Strain	Stress (MPa)	Strain	Stress (MPa)	Strain	Stress (MPa)	Strain
1	0.000	0.000	0.000	0.000	0.000	0.000	0.000	0.000
2	0.039	0.012	0.039	0.011	0.039	0.007	0.039	0.008
3	0.077	0.016	0.077	0.018	0.077	0.011	0.077	0.011
4	0.154	0.022	0.154	0.022	0.154	0.016	0.154	0.016
5	0.231	0.026	0.193	0.023	0.231	0.020	0.193	0.018
6	0.309	0.029	0.231	0.025	0.309	0.022	0.270	0.021
7	0.347	0.031	0.309	0.029	0.463	0.027	0.347	0.024
8	0.386	0.033	0.347	0.030	0.617	0.031	0.386	0.025
9	0.424	0.034	0.386	0.032	0.694	0.034	0.463	0.028

10	0.463	0.035	0.463	0.035	0.772	0.037	0.540	0.029
11	0.502	0.037	0.540	0.039	0.849	0.039	0.579	0.031
12	0.540	0.039	0.617	0.042	0.926	0.041	0.656	0.032
13	0.617	0.046	0.656	0.043	0.965	0.043	0.694	0.034
14	0.656	0.045	0.733	0.046	1.042	0.046	0.733	0.034
15	0.694	0.047	0.772	0.048	1.119	0.048	0.772	0.035
16	0.733	0.050	0.810	0.053	1.181	0.050	0.779	0.036
17	0.714	0.050	0.795	0.054	1.127	0.051	0.741	0.039
18	0.648	0.053	0.741	0.056	1.057	0.054	0.640	0.041

Table 5. Compressive strength test results of walls

Wall Sample No.	1	2	3	4	Average
Breaking Load (N)	93195	103950	151470	99990	112151.25
Compressive Strength (MPa)	0.719	0.802	1.169	0.772	0.865
Modulus of elasticity, E (MPa)	30.818	22.949	30.715	32.096	29.145

Table 6. In-plane shear test result

Description	Sample -W1	Sample -W2	Sample -W3
Plan area (mm^2)	405,000.00	405,000.00	405,000.00
Vertical load (N)	10,000.00	12,000.00	15,000.00
Horizontal load (N)	12,870.00	13,156.00	14,357.00

Normal stress (MPa)	0.0247	0.0296	0.0370
Shear stress (MPa)	0.0318	0.0325	0.0354

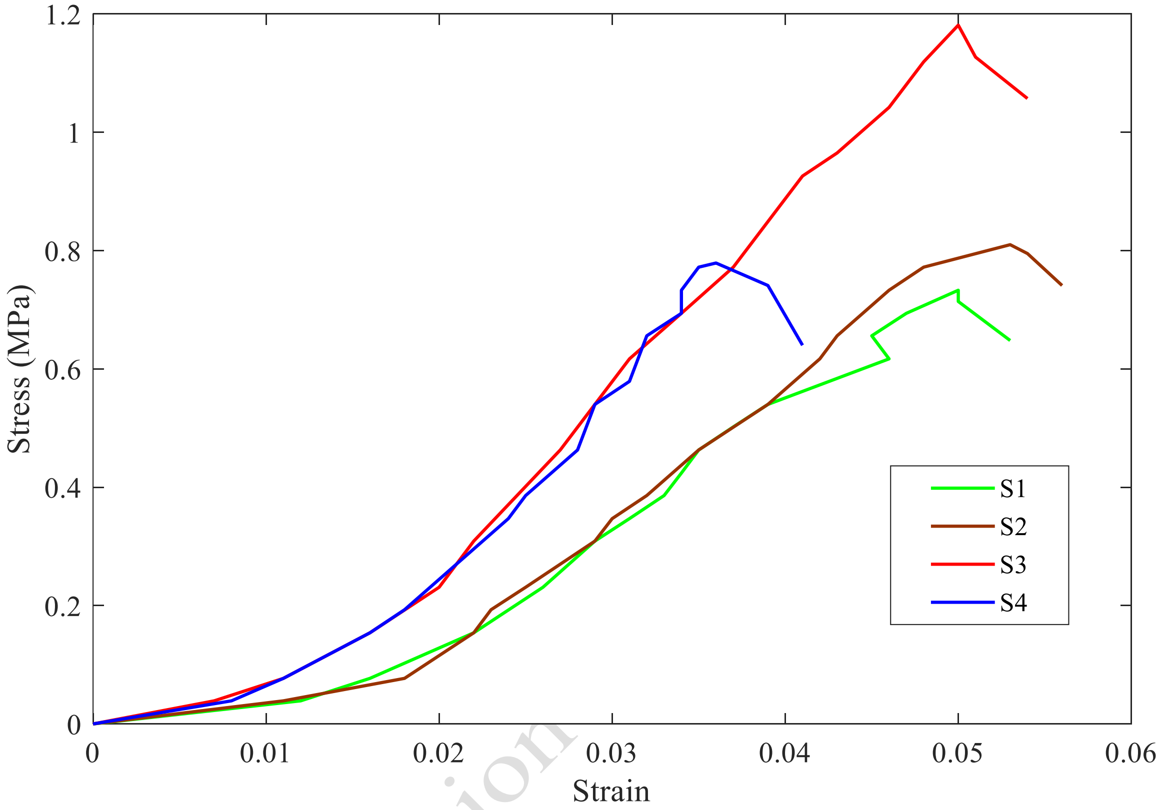

Fig. 4 Stress-strain diagram for wallet test

In-situ shear test

Shove test conducted for the replicated sample (reconstructed in laboratory using the materials of real structure) from Singh Durbar shows the average shear strength of 0.024 MPa. Adhikari et al. (Adhikari et al., 2019) reported the shear strength of 0.1 MPa for Bagh Durbar monument. The mud mortar strength was calculated by considering the vertical stress that was induced due to the dead load in the test location. Net shear strength of the brick mortar joint from the building is shown in Table 9. Mud mortar in the test locations was found to be dry, so no effect of moisture is applicable for the results reported in Table 7.

Table 7. In-situ shear test result of masonry wall

Test location	Shear stress (MPa)
Ground Floor outside pier	0.013
Ground floor front main wall	0.055
Ground floor front main wall	0.009
First floor inside wall	0.025
First floor outside wall	0.018
In-situ shear strength of mud mortar (average)	0.024

Numerical modeling and validation of test results

The mechanical properties of brick masonry obtained from experiments were validated using numerical models. We used refined Discrete Element Model (DEM) to validate the results of in-plane shear test with the previously published works (see e.g. Furukawa, Hanafusa, Kiyono, & Parajuli, 2019; Furukawa et al., 2017; Furukawa & Ohta, 2009). The refined DEM is a numerical analysis method that enables the simulation of a series of seismic behaviors from elastic to failure to collapse behavior is used (Furukawa, Kiyono, & Toki, 2011). Among numerical simulation methods, the finite element method (FEM) is the most common method for the analysis of a continuum (Zienkiewicz & Taylor, 2000). However, it has difficulty in solving failure and collapse phenomena since it is based on the mechanics of the continuum and uses a continuous shape function. A method based on dis-continuum modeling is more suitable for analyzing failure and collapse phenomena. The distinct element method (DEM) is the numerical methods for a dis-continuum developed by Cundall to solve problems in rock mechanics (Cundall & Strack, 1979). DEM models particles as rigid bodies and the interaction between two particles using a spring and dashpot. Failure is simply modeled by breaking the spring or softening the spring constant. This modeling is appropriate for failure phenomena. The disadvantage of the method is that a method for determining the spring constant from the material properties has not been established, and the values need to be quantified experimentally. Therefore, the reliability of the results is not high. The refined DEM is a refined version of the three-dimensional DEM. The point of difference from the DEM is the arrangement of springs and the spring constant being theoretically determinable from material properties. Similar to the DEM, the proposed method models the structure as an assembly of rigid elements. However, unlike the case for the DEM, the interaction between elements is modeled by multiple springs and multiple dashpots attached to the surfaces of the elements. The surface of an element is divided into many segments, and a spring and a dashpot are attached to each segment. This segmentation enables the spring constant to be derived theoretically based on the three-dimensional stress-strain relationship. Before the failure, continuous elements are connected by restoring springs, and the elastic behavior can be simulated. The failure is modeled as the breakage of the restoring springs. After the failure, the restoring springs are replaced with contact springs and dashpots. The method detects contacts and recontacts between segments, and contact forces are calculated using the contact springs and dashpots. Therefore, the method enables the simulation of elastic behavior and is suitable for simulating large displacement behaviors such as failure and collapse. In DEM approach, structure is modeled as an assembly of rigid elements, and interaction between the elements is modeled with multiple springs and multiple dashpots that are attached to the surfaces of the elements. The elements are rigid, but the method allows the simulation of structural deformation by permitting penetration between elements. Fig. 4a shows a spring for computing the restoring force (restoring spring), which models the elasticity of elements.

The restoring spring is set between continuous elements. Structural failure is modeled as breakage of the restoring spring, at which time the restoring spring is replaced with a contact spring and a contact dashpot (Fig. 4b). Fig. 4b shows the spring and dashpot for computing the contact force (contact spring and dashpot) and modeling the contact, separation, and recontact between elements. The dashpots are introduced to express energy dissipation due to the contact. Structural collapse behavior is obtained using these springs and dashpots. The elements shown in Figs. 5(a) and (b) are rectangular parallelepipeds, but the method does not limit the geometry of the elements. The surface of an element is divided into small segments as shown in Fig. 5c. The segment in the figure is rectangular, but the method does not limit the geometry of the segment. The black points indicate the representative point of each segment, and the relative displacement or contact displacement between elements is computed for these points. Such points are referred to as contact points or master points in this study. One restoring spring and one combination of contact spring and dashpot are attached to one segment (Fig. 5d) at each of the representative points in Fig. 5c. The spring constant for each segment is derived on the basis of the stress-strain relationship of the material and the segment area. Forces acting on each element are obtained by summing the restoring force, contact force, and other external forces such as the gravitational force and inertial force of an earthquake. The behavior of an element consists of the translational behavior of the center of gravity and the rotational behavior around the center of gravity. The translational and rotational behaviors of each element are computed explicitly by solving Newton's law of motion and Euler's equation of motion.

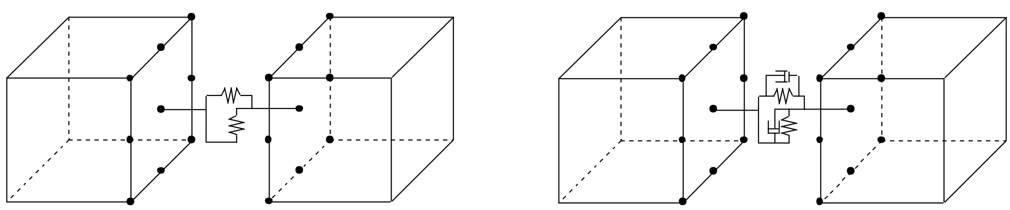

(a) (b)

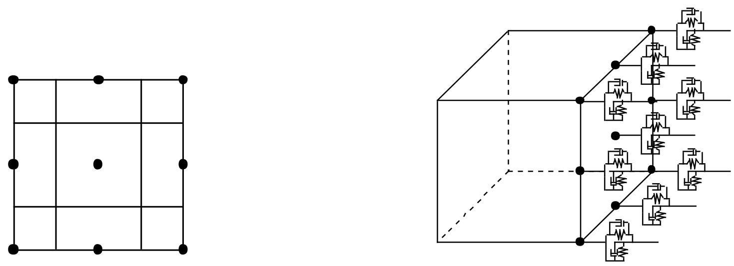

(c) (d)

Fig. 5 Basic concept of the analysis method (Furukawa et al., 2011): a) Restoring spring, b) contact spring and dashpot, c) segments and contact points, and d) multiple springs and multiple dashpots

There are two types of springs, namely restoring and contact springs. It is assumed that the spring constants of the restoring spring and those of the contact springs are the same. It is considered that each segment has its own spring. Springs are set for both the normal and shear (tangential) directions of the surface. Let us denote the area of the segment as *dA* and the relative (contact) displacement at the surface segment as un and us. The subscripts *n* an *s* indicate the values in the normal and shear directions respectively. The spring constants per area in the normal and shear directions, k_n and k_s, are obtained as follows:

$$k_n = \frac{E}{(1-\nu^2)\ell} \qquad (1)$$

$$k_s = \frac{E}{2(1+\nu)\ell} \qquad (2)$$

Where, E is Young's modulus, ν is Poisson's ratio, and ℓ is the distance from the surface at which the spring is connected to the center of gravity. In masonry structures, bricks are often connected with mortar. In this case, the spring constant per area between elements (bricks) is obtained as:

$$\bar{k}_n = \frac{1}{\frac{\ell_A - t_M/2}{E_A/(1-\nu_A^2)} + \frac{t_M}{E_M/(1-\nu_M^2)} + \frac{\ell_B - t_M/2}{E_B/(1-\nu_B^2)}} \qquad (3)$$

$$\bar{k}_s = \frac{1}{\frac{\ell_A - t_M/2}{E_A/2(1+\nu_A)} + \frac{t_M}{E_M/2(1+\nu_M)} + \frac{\ell_B - t_M/2}{E_B/2(1+\nu_B)}} \qquad (4)$$

Where, t_M is the mortar thickness, E_M is Young's modulus, and ν_M is Poisson's ratio of the mortar. The normal direction of forces is the direction perpendicular to the surface of the master point of element *A*.

The elastic behavior of structures is demonstrated by the linear multiple restoring springs between continuous elements until the restoring force of a spring reaches its elastic limit. The elastic limits are modeled using the criteria of tension, shear, and compression failure. When a spring reaches one of these limits, it is judged that failure has occurred at that segment of the spring. After the failure, the restoring spring is replaced with a contact spring and dashpot at this segment. The method can trace the expansion of failure between elements. The three failure modes, viz., tension, shear, and compression failure modes are defined.

Equations of motion can be constructed using the restoring and contact forces and other external forces. The motion of each element is obtained by solving the two equations of motion. One is the equation for the translational motion of the center of gravity, and the other is the equation for the rotational motion around the center of gravity.

$$m\ddot{\boldsymbol{x}}_g(t) + c\dot{\boldsymbol{x}}_g(t) = m\boldsymbol{g} - m\ddot{\boldsymbol{z}}(t) + \sum \boldsymbol{F}(t) \qquad (5)$$

$$\boldsymbol{I}\dot{\boldsymbol{\omega}}(t) + \boldsymbol{\omega}(t) \times \boldsymbol{I}\boldsymbol{\omega}(t) = \sum \boldsymbol{R}(t)\boldsymbol{r}(t) \times \boldsymbol{R}(t)\boldsymbol{F}(t) \qquad (6)$$

where $\mathbf{x}_g(t)$ is the displacement vector of the center of gravity of an element at time *t*, *m* is the mass of the element, *c* is the damping constant of the element, **g** is the gravitational acceleration vector, $\ddot{\mathbf{z}}_t$ is the ground acceleration vector at time *t*, and $\sum \boldsymbol{F}(t)$ is the sum of the restoring and contact force vectors at time *t*, **I** is the tensor of the moment of inertia, **r**(*t*) is the vector between the center of gravity and the point where force **F**(*t*) is applied. **R**(*t*) is the matrix representing the transformation from the absolute coordinate system to the inertial frame of reference.

The modeling approach proposed here is based on simplified micro-modeling proposed by Lourenco (1994). In the micro-modeling, individual components of the masonry structure shown in Fig. 6 (a) (i.e., brick and mortar joints) are modeled in a simple manner as shown in Fig. 6 (b). The bricks are modeled with rigid elements and the interface between elements is modeled with multiple springs and multiple dashpots. The size of one element is the sum of the brick size and mortar thickness, and the interface has zero thickness. The multiple springs and multiple dashpots interact with the surfaces of adjacent elements. The gravity centers of two adjacent elements do not change due to the failure of the mortar.

The modeling by Lourenco (1994) is based on two-dimensional finite element modeling where the elements are modeled with deformable eight-node continuum elements and mortar joints are modeled with six-node interface elements. The modeling of this study is three-dimensional, the elements are modeled with rigid rectangular parallelepipeds and hexahedrons, and the deformability of elements and the mortar joint is included in the modeling with multiple springs. Six faces surrounding the elements are divided into segments. The interval between contact points of neighboring segments is 1/4 of each edge length.

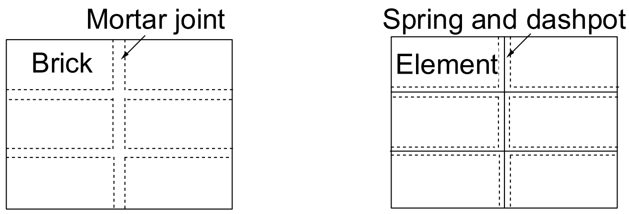

(a) (b)

Fig. 6 Analytical modeling of masonry structures: a) masonry structure, b) analytical model for the proposed method

Three-dimensional numerical analysis was performed to simulate the wall under the test loading condition using brick and mortar elements with specified input parameters.

Model wall panel represents the total setup of the test including the wooden block and metal sheets placed at the top to distribute the load uniformly. Vertical constant load in each test setup was incorporated in the steel plate weight at the top. Fig. 7 shows the failure patterns from the numerical analysis, experiment, and observed failure pattern during the 2015 Gorkha earthquake in Singh Durbar. As shown in Fig. 7, the numerical model precisely represented the experimental as well as observed failure patterns. In-plane shear test shows resemblance of the failure plane and pattern as observed in the monument during the 2015 Gorkha earthquake in Nepal. The main failure plane is brick mortar joint where brick above that plane slides and separation occurs in head joints. Overall orientation of the failure plane is diagonal from the point of loading towards the support at the bottom of another end (Fig. 7a). Results from the test and the numerical simulation using refined DEM justify the use of material properties for structural engineering applications. Shove test reported that the shear strength of the masonry from field test significantly represents the experimental result. Illampas et al. (Illampas, Ioannou, & Charmpis, 2014) highlighted that empirical manufacturing approaches lead to variability in material quality. They also noted that the properties of adobe bricks depend on the size and form of the specimen. Similarly, dynamic behavior of the adobe bricks in compression was extensively discussed by Li Piani et al. (Li Piani et al., 2020). They concluded that adobe is site dependent material and selection of mineralogical and geometrical properties of the constituents is not standardized.

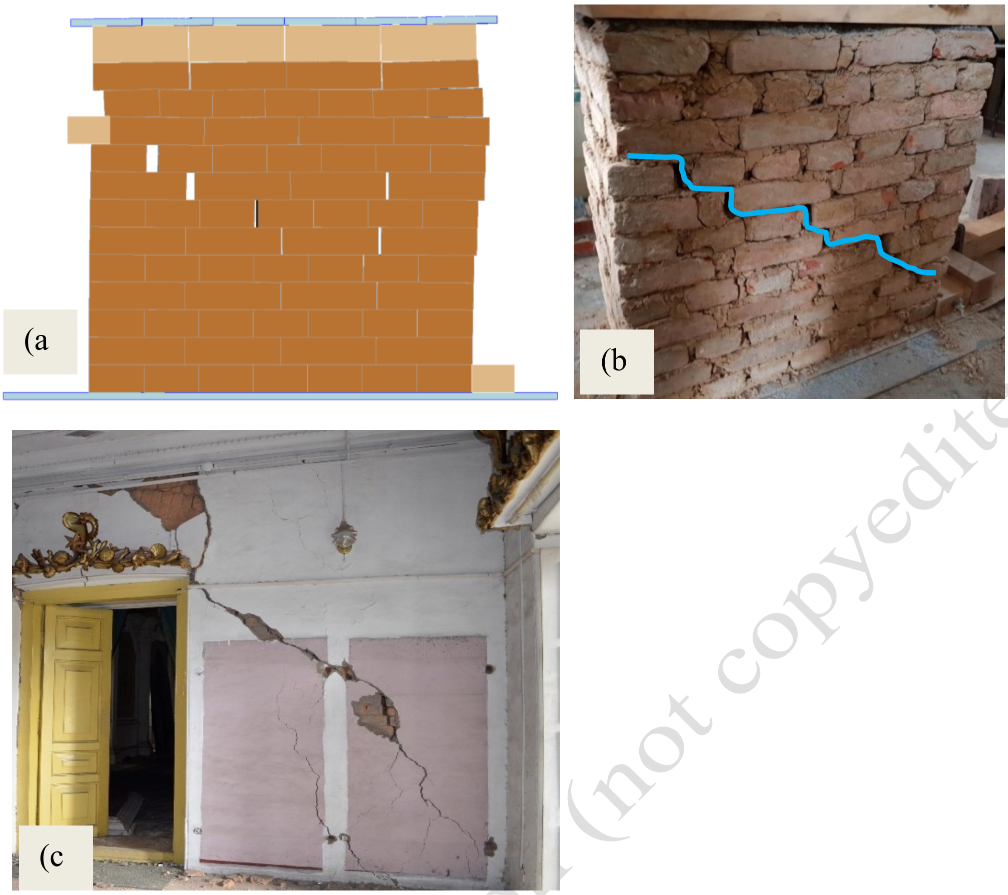

Fig. 7 a) Deformed shape with failure pattern of wall panel obtained from numerical analysis, b) major failure pattern obtained from test, c) observed damage due to the 2015 Gorkha earthquake at Singh Durbar

Conclusions

We conducted experimental testing of brick masonry in mud mortar from monumental neoclassical buildings located in Kathmandu Valley. Mechanical properties of brick units and walls are determined experimentally. The results are compared with existing test results and numerical modeling results. Brick samples from Singh Durbar monument have average compressive strength of 19.68 MPa, which is more than double the expected compressive strength of first-class brick as defined by the Nepal Building Code. Meanwhile, bricks from Shreemahal showed the compressive strength of 6.4 MPa. The average shear strength is obtained as 0.024 MPa from in-situ tests. It could be concluded that more important structures were constructed using fine quality construction materials. The mechanical properties of the monumental masonry construction in Nepal as determined in this study show that they still have appreciable and satisfactory strengths even after being used for many decades. As mechanical properties of neoclassical masonry structures are not widely reported, the results of this study may be helpful for further studies. It is common in masonry constructions to have discrepancies in mechanical properties at various locations, so we recommend the future studies to incorporate more samples to obtain the average values of parameters. Moisture content in the mortar, effect on size of frogs, variation in the manufacturing process, humidity, effects of bonding, among others can have significant impact on the properties so, these factors can be considered for further studies.

Acknowledgements

Authors would like to thank IERC Nepal, ESS Nepal, Sunita Ghimire, and Surendra Katwal for their support during the lab and field experiments.

References

Adhikari, R., Jha, P., Gautam, D., & Fabbrocino, G. (2019). Seismic Strengthening of the Bagh Durbar Heritage Building in Kathmandu Following the Gorkha Earthquake Sequence. *Buildings*, *9*(5), 128. https://doi.org/10.3390/buildings9050128

Ahmad, N., Ali, Q., Ashraf, M., Alam, B., & Naeem, A. (2012). Seismic vulnerability of the Himalayan half-dressed rubble stone masonry structures, experimental and analytical studies. *Natural Hazards and Earth System Sciences*. https://doi.org/10.5194/nhess-12-3441-2012

Ahmad, N., Ali, Q., & Umar, M. (2012). Simplified engineering tools for seismic analysis and design of traditional Dhajji-Dewari structures. *Bulletin of Earthquake Engineering*. https://doi.org/10.1007/s10518-012-9364-9

Ali, Q., Khan, A. N., Ashraf, M., Ahmed, A., Alam, B., Ahmad, N., … Umar, M. (2013). Seismic performance of stone masonry buildings used in the Himalayan belt. *Earthquake Spectra*. https://doi.org/10.1193/091711EQS228M

Barluenga, G., Estirado, F., Undurraga, R., Conde, J. F., Agua, F., Villegas, M. Á., & García-Heras, M. (2014). Brick masonry identification in a complex historic building, the Main College of the University of Alcalá, Madrid (Spain). *Construction and Building Materials*. https://doi.org/10.1016/j.conbuildmat.2013.12.027

Boschi, S., Galano, L., & Vignoli, A. (2019). Mechanical characterisation of Tuscany masonry typologies by in situ tests. *Bulletin of Earthquake Engineering*. https://doi.org/10.1007/s10518-018-0451-4

Bureau of Indian Standards. IS 3495-1 to 4 (1992): Methods of tests of burnt clay building bricks (1992).

Central Bureao of Statistics. (2012). *National Population and Housing Census 2011 (National Report) Government of Nepal* (Vol. 01).

Costigan, A., Pavía, S., & Kinnane, O. (2015). An experimental evaluation of prediction models for the mechanical behavior of unreinforced, lime-mortar masonry under compression. *Journal of Building Engineering*, *4*, 283–294. https://doi.org/10.1016/j.jobe.2015.10.001

Cundall, P. A., & Strack, O. D. L. (1979). A discrete numerical model for granular assemblies. *Geotechnique*. https://doi.org/10.1680/geot.1979.29.1.47

Formisano, A., Vaiano, G., Fabbrocino, F., & Milani, G. (2018). Seismic vulnerability of Italian masonry churches: The case of the Nativity of Blessed Virgin Mary in Stellata of Bondeno. *Journal of Building Engineering*. https://doi.org/10.1016/j.jobe.2018.07.017

Furukawa, A., Hanafusa, R., Kiyono, J., & Parajuli, R. R. (2019). Investigation of Natural Frequency Reduction Mechanism of a Historic Masonry Building in Patan following the 2015 Gorkha Earthquake in Nepal. *Journal of Japan Association of Earthquake Engineering*, *19*(2), 70–86.

Furukawa, A., Kiyono, J., Parajuli, R. R., Parajuli, H. R., & Toki, K. (2017). Evaluation of Damage to a Historic Masonry Building in Nepal through Comparison of Dynamic Characteristics before and after the 2015 Gorkha Earthquake. *Frontiers in Built Environment*, *3*(October). https://doi.org/10.3389/fbuil.2017.00062

Furukawa, A., Kiyono, J., & Toki, K. (2011). Proposal of a numerical simulation method for elastic, failure and collapse behaviors of structures and its application to seismic response analysis of masonry walls. *Journal of Disaster Research*. https://doi.org/10.20965/jdr.2011.p0051

Furukawa, A., & Ohta, Y. (2009). Failure process of masonry buildings during earthquake and associated casualty risk evaluation. *Natural Hazards*, *49*(1), 25–51. https://doi.org/10.1007/s11069-008-9275-x

Gautam, D. (2017). Seismic Performance of World Heritage Sites in Kathmandu Valley during Gorkha Seismic Sequence of April-May 2015. *Journal of Performance of Constructed Facilities*, *31*(5). https://doi.org/10.1061/(ASCE)CF.1943-5509.0001040

Gautam, D. (2018). Observational fragility functions for residential stone masonry buildings in Nepal. *Bulletin of Earthquake Engineering*. https://doi.org/10.1007/s10518-018-0372-2

Gautam, D., & Rodrigues, H. (2018). Seismic Vulnerability of Urban Vernacular Buildings in Nepal: Case of Newari Construction. *Journal of Earthquake Engineering*. https://doi.org/10.1080/13632469.2018.1498411

Illampas, R., Ioannou, I., & Charmpis, D. C. (2014). Adobe bricks under compression: Experimental investigation and derivation of stress-strain equation. *Construction and Building Materials*. https://doi.org/10.1016/j.conbuildmat.2013.11.103

Jafari, S., Rots, J. G., Esposito, R., & Messali, F. (2017). Characterizing the Material Properties of Dutch Unreinforced Masonry. *Procedia Engineering*, *193*, 250–257. https://doi.org/10.1016/j.proeng.2017.06.211

Jha, P., Motra, G., Sah, B. K., Adhikari, R., & Gautam, D. (2019). Seismic vulnerability assessment and retrofitting of Bal Mandir building. In *International Conference on Health Engineering in Disaster*. Pokhara, Nepal.

Kaushik, H. B., Rai, D. C., & Jain, S. K. (2007). Stress-strain characteristics of clay brick masonry under uniaxial compression. *Journal of Materials in Civil Engineering*. https://doi.org/10.1061/(ASCE)0899-1561(2007)19:9(728)

Li Piani, T., Weerheijm, J., Peroni, M., Koene, L., Krabbenborg, D., Solomos, G., & Sluys, L. J. (2020). Dynamic behaviour of adobe bricks in compression: The role of fibres and water content at various loading rates. *Construction and Building Materials*. https://doi.org/10.1016/j.conbuildmat.2019.117038

Lourenco, P. B. (1994). *Analysis of masonry structures with interface elements, theory and applications*. Delft University of Technology, Faculty of Civil Engineering.

Lumantarna, R., Biggs, D. T., & Ingham, J. M. (2014a). Compressive, flexural bond, and shear bond strengths of in situ New Zealand unreinforced clay brick masonry constructed using lime mortar between the 1880s and 1940s. *Journal of Materials in Civil Engineering*, *26*(4), 559–566. https://doi.org/10.1061/(ASCE)MT.1943-5533.0000685

Lumantarna, R., Biggs, D. T., & Ingham, J. M. (2014b). Uniaxial compressive strength and stiffness of field-extracted and laboratory-constructed masonry prisms. *Journal of Materials in Civil Engineering*, *26*(4), 567–575. https://doi.org/10.1061/(ASCE)MT.1943-5533.0000731

Milosevic, J., Gago, A. S., Lopes, M., & Bento, R. (2013). Experimental assessment of shear strength parameters on rubble stone masonry specimens. *Construction and Building Materials*. https://doi.org/10.1016/j.conbuildmat.2013.06.036

Parajuli, R. R. (2020). Features and seismic response of large masonry structures: A Case study of Singh Durbar main building, Nepal. In R. Rupakhety & D. Gautam (Eds.), *Masonry Construction in Active Seismic Regions*. Elsevier.

Parajuli, R. R., & Kiyono, J. (2015). Ground motion characteristics of the 2015 gorkha earthquake, survey of damage to stone masonry structures and structural field tests. *Frontiers in Built Environment*. https://doi.org/10.3389/fbuil.2015.00023

Potenza, F., Federici, F., Lepidi, M., Gattulli, V., Graziosi, F., & Colarieti, A. (2015). Long-term structural monitoring of the damaged Basilica S. Maria di Collemaggio through a low-cost wireless sensor network. *Journal of Civil Structural Health Monitoring*. https://doi.org/10.1007/s13349-015-0146-3

Rahgozar, A., & Hosseini, A. (2017). Experimental and numerical assessment of in-plane monotonic response of ancient mortar brick masonry. *Construction and Building Materials*, *155*, 892–909.

https://doi.org/10.1016/j.conbuildmat.2017.08.079

Sarangapani, G., Reddy, B. V. V., & K. S., J. (2005). Brick-Mortar Bond and Masonry Compressive Strength. *Journal of Materials in Civil Engineering*, *17*(2), 229. https://doi.org/10.1061/(ASCE)0899-1561(2005)17:2(229)

Tamrakar, A., & Parajuli, R. R. (2019). Conservation of Cultural Heritage: Issues along Thapathali – Teku stretch of the Bagmati River in Kathmandu valley. *Heritage*, *2*(3).

Zienkiewicz, O. C., & Taylor, R. L. (2000). *The Finite Element Method*. Oxford: Butterworth Heinemann.